Journal of Oceanography
https://doi.org/10.1007/s10872-024-00721-z

ORIGINAL ARTICLE

Sea ice-melt amount estimated from spring hydrography in the Sea of Okhotsk: spatial and interannual variabilities

Mariko Honda[1] · Kay I. Ohshima[1,2,3,4] · Vigan Mensah[2] · Jun Nishioka[1,3,4] · Masatoshi Sato[5] · Stephen C. Riser[6]

Received: 1 October 2023 / Revised: 9 April 2024 / Accepted: 12 April 2024

Abstract

This study provides the first estimation of sea ice-melt amount in the Sea of Okhotsk based on spring hydrographic data accumulated for nearly a hundred years. Just after sea ice melts completely, a low-salinity layer appears on the ocean surface, overlying the layer of Winter Water at the freezing point. The integration of the salinity decrease from Winter Water should correspond to the total ice-melt amount. We developed an algorithm to extract the profiles that clearly show the salinity deficit and converted the salinity deficit to the ice-melt amount from all available data. The climatological map shows that ice-melt amount decreases toward the ice edge and exhibits large values around the northern Sakhalin Island, reflecting the ice thickness distribution. In the southern area (south of 48°N), where sea ice is transported from the north, the average ice-melt amount is estimated to be ~ 71 cm in thickness. It is clearly shown that the ice-melt amount has decreased by ~ 30% in the southern area since the 1990s. These changes possibly affect the regional climate through the decreased latent heat of sea ice and potentially affect biological production through weakened stratification caused by decreased ice melt. We also suggested that ice-melt amount did not show a significant trend during the 1930s–1970s, implying that our methodology could extract information on sea ice before the era of satellite observations.

Keywords Sea ice melt · Sea of Okhotsk · Seasonal ice zone · Global warming · Freshwater flux

1 Introduction

The Sea of Okhotsk is the marginal sea of the North Pacific and the southernmost sea with a sizable seasonal sea ice cover in the Northern Hemisphere. The Sea of Okhotsk is located downwind of the coldest region in the Northern Hemisphere (Nihashi et al. 2009). In winter, the prevailing northwesterly winds bring very cold air mass over the Sea of Okhotsk. The associated large amount of heat loss to the atmosphere causes high sea ice production. In particular, the coastal polynya in the northwestern shelf has the largest ice production in the Northern Hemisphere (Ohshima et al. 2016). The sea ice produced in the northwest region is advected to the south by the prevailing northwesterly winds and the East Sakhalin Current (ESC) (Simizu et al. 2014). Sea ice formation begins over the northwestern shelf at the end of November, and ice extent reaches its maximum at the end of February or the beginning of March. The melting and retreat of sea ice starts in the south in March, and all of the sea ice in the Sea of Okhotsk melts by the end of June.

In the central and northern parts of the sea, cyclonic circulation is dominant with a strong southward flow of the ESC along Sakhalin Island (Mizuta et al. 2003). The ESC consists of two branches, nearshore and offshore branches (Ohshima et al. 2002). The nearshore branch is mainly driven by the alongshore wind stress (Simizu and Ohshima 2006). The nearshore branch also includes a component that is a surface intensified current during summer and fall due to the freshwater flux from the Amur River (Mizuta et al.

✉ Mariko Honda
marikoh@ees.hokudai.ac.jp

1 Graduate School of Environmental Science, Hokkaido University, Sapporo, Hokkaido, Japan

2 Institute of Low Temperature Science, Hokkaido University, Sapporo, Hokkaido, Japan

3 Arctic Research Center, Hokkaido University, Sapporo, Hokkaido, Japan

4 Pan-Okhotsk Research Center, Institute of Low Temperature Science, Hokkaido University, Sapporo, Hokkaido, Japan

5 Wakkanai Fisheries Research Institute, Hokkaido Research Organization, Wakkanai, Hokkaido, Japan

6 School of Oceanography, University of Washington, Seattle, WA, USA

Published online: 11 May 2024

2003). The offshore branch can be regarded as the western boundary current of the cyclonic circulation driven by a positive wind stress curl (Ohshima et al. 2004) Both branches exhibit the strong seasonal variation, from a maximum transport in winter to a minimum transport in summer. In the southern part of the sea with the deep Kuril Basin, the mean flow field is a weak anticyclonic circulation (Mensah et al. 2019), with the dominance of mesoscale eddy (Bulatov et al. 1999; Ohshima et al. 2002), which can often be visualized as ice-ocean eddies in the ice-covered season (Wakatsuchi et al. 1990).

Exchange of waters between the Okhotsk Sea and the North Pacific occurs through the Kuril Straits, with intensification in winter (Ohshima et al. 2010; Kida and Qiu 2013; Prants et al. 2015). Then, relatively warm water originating from the Bering Sea flows into the eastern part of the Okhotsk Sea (Andreev and Pipko 2022). This inflow prohibits the eastward extension of the sea ice cover, and its interannual variability partly controls the sea ice extent in the Okhotsk Sea (Nakanowatari et al. 2010).

In general, sea-ice production, transport, and melt play the roles of salt/freshwater and heat transports. In the Sea of Okhotsk, a large amount of sea ice produced in the northern coastal polynyas is transported to the southern part of the sea, absorbing latent heat when the sea ice melts, resulting in negative southward heat transport (Nihashi et al. 2012). This negative heat transport to the south induces a cold regional climate in the northern and eastern parts of Hokkaido (Ohshima et al. 2003). In this sea, sea ice is melted mainly by ocean heat warmed by solar radiation through the open-water fraction (Nihashi et al. 2011).

Seasonal sea ice zones, such as the Sea of Okhotsk, provide rich biological resources, mainly originating from large phytoplankton blooms associated with sea-ice melt (hereafter referred to as spring blooms). Kishi et al. (2021) quantified the relationship between the melting of sea ice and biological production by estimating net community production (NCP) in the Sea of Okhotsk based on the oxygen increase from the profiling floats. They found that the NCP for the case in which sea ice existed immediately before the phytoplankton bloom (the prior-ice case) was ~ 3 times higher than that for the non-ice case. The relationship between sea-ice melt and spring bloom has also been suggested from satellite observations in the Sea of Okhotsk (Nihashi et al. 2012). In the southern part of the Okhotsk Sea, the chlorophyll-a concentration reaches its maximum in April, probably because of the melting of sea ice transported from the northern shelves (Kuga et al. 2023). The freshwater supply associated with sea-ice melt intensifies surface stratification, which provides a favorable condition for the increase in phytoplankton through enhanced light availability (Sorokin and Sorokin 1999). In addition, micronutrient, such as iron released from sea ice, and ice algae are considered to contribute to the prominent spring bloom (Kanna et al. 2014, 2018; Yan et al. 2020).

In the northern coastal polynyas, active ice production generates cold high salinity water through brine rejection, leading to the formation of Dense Shelf Water. The Dense Shelf Water is ventilated to the intermediate layer, driving the intermediate overturning circulation that extends to the North Pacific (Talley 1991; Shcherbina et al. 2003). In contrast, sea ice melting supplies freshwater to the southern part when sea ice is transported from the north. A low–salinity layer then appears on the ocean surface in spring. The discharge of the Amur River also supplies a significant amount of freshwater to the western part of the sea. The importance of salt/freshwater and heat transports with ice production/melt in the Okhotsk Sea was also suggested by a coupled ice-ocean model (Watanabe et al. 2004). Nihashi et al. (2012) made the first trial to estimate the salt/freshwater and heat transports associated with ice production/melt, using the sea ice products by the satellite microwave radiometer and atmospheric data from the ERA-Interim re-analysis.

In the past 50 years, air temperature in the upwind region of the Sea of Okhotsk in fall and winter has increased by 2 °C, which is approximately three times the global average (e.g. Nakanowatari et al. 2007). Kashiwase et al. (2014) showed a significant decreasing trend of sea ice production in the northern polynyas, which can be explained mainly by such a warming trend. The reduction in ice production has resulted in prominent freshening and a decrease of Dense Shelf Water over the northern shelves of the Okhotsk Sea, finally leading to the weakening of the intermediate overturning circulation in the North Pacific (Ohshima et al. 2014; Mensah and Ohshima 2021). Although the maximum sea ice area in the whole Sea of Okhotsk had a decreasing trend of 21% for the past 45 years (1979–2023), the era of satellite observation, its year-to-year or decadal variability is also large (https://www.data.jma.go.jp/gmd/kaiyou/shindan/a_1/series_okhotsk/series_okhotsk.html).

Regarding sea-ice production in the Sea of Okhotsk, there have been a series of quantitative estimations using satellite passive microwave data and heat flux calculations (Nihashi et al. 2009, 2012; Kashiwase et al. 2014; Nakata and Ohshima 2022). In contrast, very few quantitative studies have been conducted on the melting of sea ice. Estimating the ice–melt amount is difficult because the melting processes occur unevenly from the side and bottom of the ice floe or through the brash ice. The only estimation study of the ice-melt amount is Nihashi et al. (2012), who calculated the ice-melt amount so that it is balanced with sea-ice production in the whole Sea of Okhotsk using satellite passive microwave data and heat budget analysis. However, their treatments of ice-melt amount were rough based on ad-hoc assumptions such that the ice-melt amount was calculated

by the decrease in sea ice area with a constant ice thickness over the entire Sea of Okhotsk.

We regard estimating the ice-melt amount from the measurement of sea ice as difficult at this stage. However, such ice-melt estimates may be possible from the analysis of seawater properties just after the end of the melting season. Immediately after the sea ice melts, a low-salinity layer appears on the ocean surface, overlying Winter Water (WW) at the freezing point. The integration of the salinity decrease from WW should correspond to the total amount of sea-ice melt. In this study, we focus on this fresh surface layer to estimate the ice-melt amount. Particularly in the southern part of the Okhotsk Sea, hydrographic observations were conducted in spring even before the era of satellite sea ice observation, which will enable the examination of long-term variations in ice-melt amount.

In this study, we developed an algorithm that extracts temperature/salinity profiles showing the effect of ice melting clearly and estimated the ice-melt amount using the salinity deficit in the surface layer. We then created a climatology map of the ice-melt amount in the Sea of Okhotsk. Finally, we discuss the interannual variability of the ice-melt amount, combined with the analysis of changes in spring hydrography in the southern area of the Okhotsk Sea, where a relatively large amount of data exists.

2 Data

Hydrographic data have been acquired in the Sea of Okhotsk for nearly a hundred years. In this study, we used the temperature and salinity profile data in the upper 200 m layer taken from February to July. There are three sources for in-situ observations: ship-based observations, profiling float observations, and biologging. Ship-based observation data were derived from the World Ocean Database 2018 (WOD18) (Boyer et al. 2018) and the Japan Oceanographic Data Center (JODC). In addition, we used shipboard CTD/XCTD data from the Russian R/V Khromov (Kh10) from the Far Eastern Regional Hydrometeorological Research Institute, the Japanese R/V Hokuyo-maru from the Wakkanai Fisheries Research Institute, the R/V Shinsei-maru (KS-21–6 and KS-22–6) from the Japan Agency for Marine-Earth Science and Technology, and other Japanese cruises that have not yet been archived in WOD18 or JODC. We also used profiling float data derived from 29 floats deployed in the Sea of Okhotsk as part of the joint Japan-Russia-U.S. study (Ohshima et al. 2005) and of the cooperative study between Hokkaido University and the University of Washington (Ohshima et al. 2010, 2014). Profiling floats have the advantage of obtaining hydrographic data with a 5- or 10-day cycle continuously just after the sea-ice melt. Biologging data were obtained from the CTD tags attached to six seals and sea lions (Nakanowatari et al. 2017).

Sea ice concentration (SIC) is the key quantity for various discussions and was also used to check the existence of sea ice for observational locations. The SIC data were derived from two satellite passive microwave radiometers: Scanning Multichannel Microwave Radiometer (SMMR) with a temporal resolution of approximately two days for 1978–1987 and the daily Special Sensor Microwave-Imager (SSM/I) from 1987 to the present, provided by the National Snow and Ice Data Center (NSIDC). The Bootstrap algorithm (Comiso 1995) was used for SIC estimation. Lastly, to create the gridded data set of ice-melt amount by taking account of the bathymetry (Sect. 3), we used the bathymetry data of the Sea of Okhotsk from ETOPO1 with a grid spacing of one minute, provided by the National Geophysical Data Center.

3 Methods

3.1 Extraction of the profiles for ice-melt estimation

In the Sea of Okhotsk, WW layer at the freezing point (~ − 1.7 °C) is formed from the surface in ice-covered areas by severe cooling, wind stirring, and ice formation. The vertically uniform WW layer sometimes extends 200–300 m in the southern part of the Okhotsk Sea (Ohshima et al. 2001). When air temperature and solar radiation increase in spring, sea ice is melted by heat in the upper ocean heated mainly by solar radiation (Nihashi et al. 2011). Thereby, warmed and freshened water appears in the surface layer overlying the vertically uniform WW layer. Then the integration of the salinity decrease in this surface-freshened layer from the WW salinity corresponds to the total amount of sea-ice melt.

In this study, we developed an algorithm to detect the bottom of this surface layer (top of the WW layer) to estimate the ice-melt amount from the salinity deficit. The ice-melt amount estimated in this study is for the melting during the ice retreat season. Even during the ice-advance season, sea ice melts around the ice edge (Watanabe et al. 2004). Such melting is not included in our estimations because we focus on the season after all the sea ice has melted away (Fig. 1).

First, we extracted profiles that clearly show the salinity deficit among all spring hydrographic data. An idealized profile is the case in which the warmed, freshened surface water is distinctly separated from the underlying WW at the freezing temperature, as typically shown in Fig. 2a. This type of profile is categorized as Type A in this study. Soon after the sea ice melts completely, the underlying WW layer remains vertically uniform, with the salinity of WW unchanged. Over time, the vertically uniform WW layer would be eroded by mixing with the warmed, freshened surface water from the

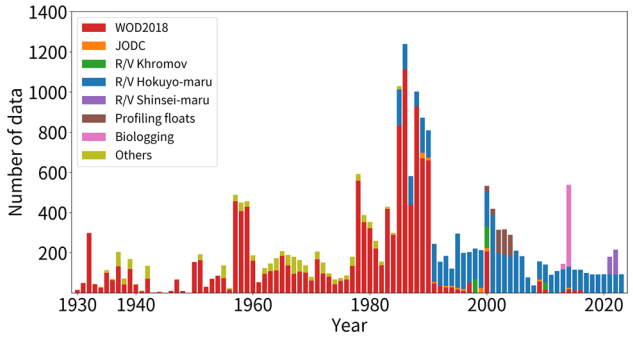

Fig. 1 Time series of the number of temperature/salinity profiles obtained in the Sea of Okhotsk during February–July. The data sources are indicated by different colors depicted in the legend at the upper left. See the text for the abbreviations in the legend. It is noted that only 12% of all the spring hydrographic data shown here was used for estimation of ice-melt amount

top, and with warmer saline water from the deeper layer. Then, a temperature minimum occurs as a remnant of WW, as typically shown in Fig. 2b. If this minimum temperature is sufficiently close to the freezing temperature, only the surface layer above this minimum is likely affected by ice melting. Such a profile with the minimum temperature of < -1 °C is categorized as Type B. When the mixing further progresses, a clear remnant of the WW that remained near the freezing temperature disappears, as typically shown in Fig. 2c. Such a profile cannot be used to estimate the ice-melt amount. We conservatively extracted the profiles of Types A and Type B to exclude the profiles with ambiguity for the estimation. We used only 12% of the data among all the spring hydrographic data through severe screening, as will be described later. The appendix describes the details of the algorithm used to extract the profiles of Types A and B and to identify the deepest depth affected by ice melting.

The initially collected data include some observations in the ice-covered area with sea ice not being melted completely and some observations in the area with no sea-ice cover during the previous winter. To exclude such data, we used the time series of the daily SIC averaged over a radius of 25 km from the observational location. If the following two conditions are satisfied, that profile is judged to be used for the estimation of sea-ice melt.

A. The daily SIC exceeded 50% at least once during the preceding winter.

B. The elapsed time since the final day when the daily SIC exceeded 15% ranges between 5 and 100 days.

As SIC data are only available after November 1978, we used the SIC averaged over 1978–1989 for each gridded cell to check the sea ice conditions for ice-melt estimation before 1978.

Along the Hokkaido coast, relatively warm, saline water from the Japan Sea flows as the Soya Warm Current (SWC) (e.g., Ohshima et al. 2017). We excluded the areas affected by the SWC for estimation of sea-ice melt because the ice-melt amount cannot be adequately estimated under the influence of such a water mass. Specifically, we excluded all data taken in the region with a depth of < 100 m south of 45° N.

3.2 Calculation of the ice-melt amount

The average of salinity deficit (ΔS) from the surface to the deepest depth affected by the melting (Z_0) is calculated as follows:

$$\Delta S = \frac{\int_0^{Z_0} (S_{z0} - S(z)) dz}{Z_0}, \quad (1)$$

where $S(z)$ is salinity at each depth and S_{z_0} is the salinity at Z_0.

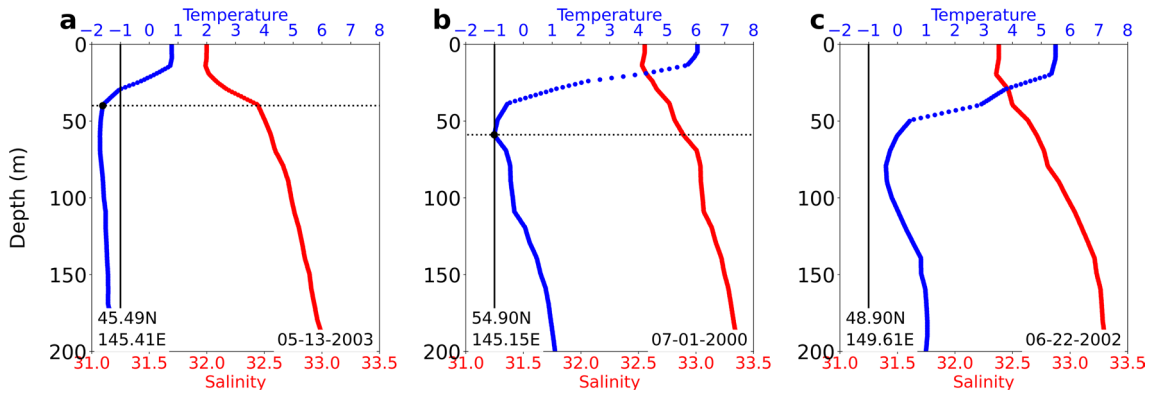

Fig. 2 Examples of vertical profiles of temperature (blue lines) and salinity (red lines) after sea ice melt. The profiles of Type A (**a**) and Type B (**b**) were used to estimate the ice-melt amount, whereas profile **c** was not used. The black vertical line indicates the temperature of − 1.0 ℃. The dotted lateral lines in **a** and **b** indicate the deepest depth affected by sea-ice melt. The latitude and longitude of the observational location are shown in the lower left. The observation date is shown on the lower right

Using ΔS, ice-melt amount x in thickness is given by:

$$x = \frac{\rho_w}{\rho_i} \frac{\Delta S}{(S_{z0} - \Delta S - S_i)} Z_0, \tag{2}$$

where the densities of sea ice (ρ_i) and sea water (ρ_w) are set to 900(kg/m^3), and 1025(kg/m^3), respectively. The salinity of sea ice (S_i) is set to 4.6 psu, according to Toyota et al. (2007). Similar estimation of sea-ice melt from the salinity deficit was made in the Weddell Sea in the Southern Ocean by Martinson and Iannuzzi (1998).

3.3 Creation of the gridded map of the ice-melt amount

To create a gridded map of the ice-melt amount, we used the shrinking and stretching constraint integrated (SSCI) scheme as a weighting function (Mensah and Ohshima 2023; Shimada et al. 2017). This scheme reflects how the water masses and sea ice tend to follow the bottom contours in the Sea of Okhotsk when the stratification is relatively weak during spring. This property originates in the conservation of potential vorticity, which is the basis of the SSCI scheme. This scheme uses a water column shrinking and stretching constraint in addition to a distance constraint to map observations into a gridded domain, represented by the following weight function.

$$W(r,\ \Delta h) = \exp\left[\left(\frac{r}{L_r}\right)^2 - \left(\frac{\phi}{L_\phi}\right)^2\right], \tag{3}$$

where r is the horizontal distance between the observational point and the grid center point. The shrinking/stretching parameter $\phi(= \Delta h/h)$ is given as follows. The value h represents the bottom depth at the grid center point and the value Δh is the difference between h and the bottom depth at the observational point. Using bilinear interpolation, the bottom depths of the grid center point and observational point are calculated from the ETOPO-1 min bathymetry data of the four surrounding points. The horizontal decorrelation scale (L_r) is set to 97 km, and the decorrelation scale of shrinking/stretching parameter L_ϕ is set to 0.56, according to the estimation in the Sea of Okhotsk by Mensah and Ohshima (2023).

The size of a grid cell is set to be 1/3° in latitude and 1/2° in longitude. We set the initial search radius to 1.5 times L_r (145 km) from each grid center point. If the number of observations within the search radius was less than five for a certain grid point, the search radius was increased to 2 times L_r (194 km). If the number of observations by this extension of the search radius was still less than five, that grid point was regarded as having no data.

3.4 Sea-ice extent defined from the SIC data

If the ice-melt amount is estimated in a large ice-extent year at an area that is not covered with sea ice in a normal ice-extent year, the gridded dataset would count this estimation. Therefore, the ice-melt area tends to be overestimated. To create a less-biased climatology of ice melting, we define the average ice-extent based on long-term SIC data. For the past 44 years (1979–2022), we first determine the day when the integrated SIC over the entire Okhotsk Sea becomes maximum for each year and define the yearly maximum ice-extent area as the integration of areas with SIC of > 15% on that day. Next, we calculated the frequency at which the yearly maximum ice-extent area occupies each grid point in the 44 years. For example, 25% of the frequency means that the yearly maximum ice-extent area includes that grid point 11 times in 44 years. Figure 3 shows the distribution of the frequency of the maximum ice extent. Finally, we defined the area with a frequency of > 25% as the average ice-extent in the Sea of Okhotsk.

4 Results

4.1 Estimated ice-melt amount

First, we present how the temperature and salinity profiles evolve after sea ice melts and how such evolution affects the estimation of the ice-melt amount by showing a time series of their vertical profiles taken from a profiling float, as an example (Fig. 4). Although the salinity profile is diffused (Fig. 4b) and the temperature is increased (Fig. 4a) gradually in the surface freshened layer formed by sea-ice melt, as time goes by, the salinity deficit can be identified from our algorithm for nearly three months (Fig. 4d) after sea ice melts away (Fig. 4c). In this case, the estimated ice-melt amount is 52 cm on average with a standard deviation (SD) of 12 cm from nine profiles at 10-day intervals. A relatively small SD suggests that the ice-melt amount can be adequately estimated to some extent from profiles taken 2–3 months after sea ice melts away, if strong mixing does not occur in the surface layer.

Through the extraction algorithm of Type A and Type B profiles and other screening using SIC and bathymetric data, a total of 2559 profiles were used to estimate the ice-melt amount. This number is only12% of all spring data ($n = 21{,}735$) initially collected in the Sea of Okhotsk. This results from our conservative approach that reliability is more important than data increase. Figure 5 shows the plots of the sea ice-melt amount estimated from all profiles in which the salinity deficit is detectable.

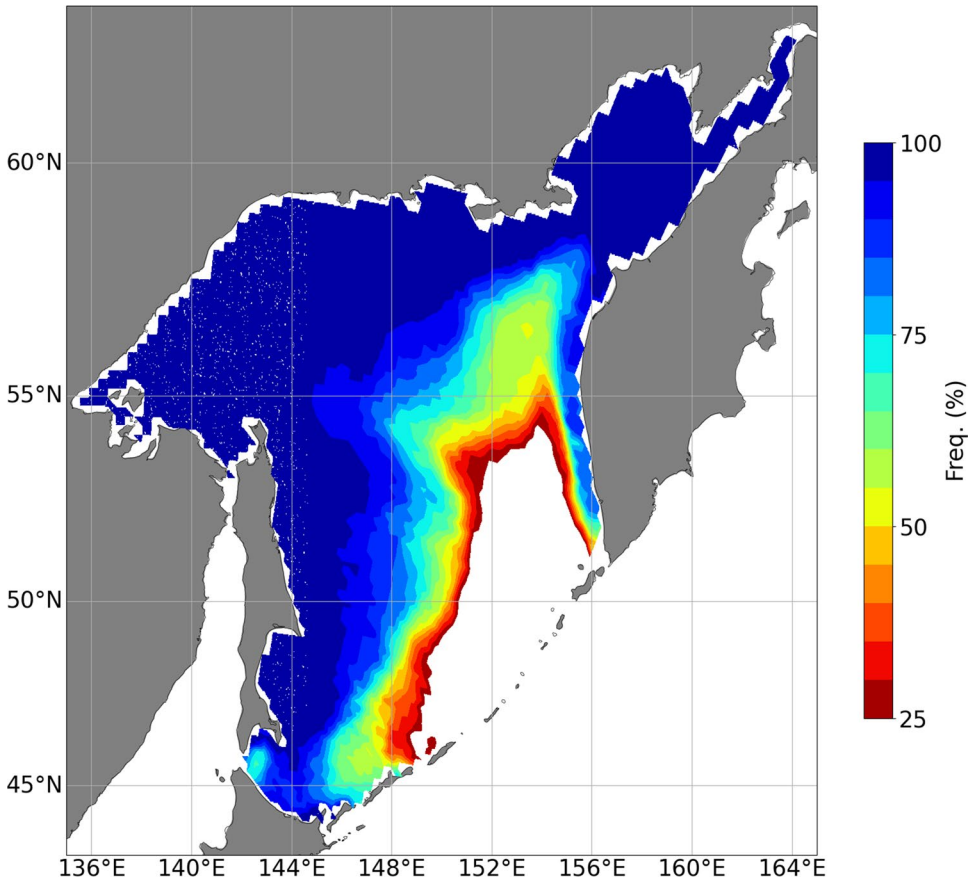

Fig. 3 Climatology map of the frequency of maximum sea-ice extent in the Sea of Okhotsk over the past 44 years

4.2 Gridded map of the ice-melt amount

Although the number of the estimated data is greatly reduced from the initially collected data, we obtained sufficient data to map the ice-melt amount for the entire Sea of Okhotsk. Based on 2559 estimations, we created a gridded map of the ice-melt amount (Fig. 6) using the SSCI scheme described in Sect. 3. The map shows that the ice-melt amount decreases toward the east or the ice edges. The most prominent feature is that the area of large ice-melt amount is distributed around northern Sakhalin Island, with melt thickness values of 120–150 cm. The area north of Sakhalin Island corresponds to high ice convergent area, where active ice thickening by rafting and ridging is expected (Kimura and Wakatsuchi 2004). It is also noted that the surface freshwater in this region partly contains the Amur River discharge as will be discussed in Sect. 6. Nihashi et al. (2018) estimated the spatial distribution of sea-ice thickness in the Sea of Okhotsk for the 5 years from 2003 to 2008 from Ice, Cloud, and land Elevation Satellite (ICESat) data. The ice thickness determined by Nihashi et al. (2018) was the thickness averaged throughout the winter. In principle, the ice thickness distribution does not necessarily correspond to the ice-melt amount distribution because of advection of sea ice. Even so, the overall distributions of ice thickness and ice-melt amount show similar spatial features (see Fig. S1 and Fig. 7 in Nihashi et al. (2018)): large values around northern Sakhalin Island, small values over the northern shelves, and an eastward decrease to the ice edges. These imply that the ice-melt amount reflects the local ice thickness to some extent. However, the thickness derived from the ICESat data tends to be larger than the ice-melt amount. It should be noted that the estimation of ice thickness from the ICESat data contains a relatively large uncertainty in the Sea of Okhotsk due to the lack of basic information, such as the snow cover ratio on sea ice.

4.3 Error evaluation of the gridded data

As shown in Fig. 5, the estimated ice-melt data are sparse in some areas. Here, the reliability of the gridded data was quantified using the root mean square error (RMSE) at the 95% confidence interval (e_{95}) for each grid cell assuming a normal distribution, represented as

$$e_{95} = 1.96 \times \frac{1}{\sqrt{N}} \sqrt{\frac{\sum_{i=1}^{N} (x-di)^2}{N}}, \tag{4}$$

where x is the value of the ice-melt amount for each grid cell, di is the ice-melt amount estimated from an individual profile satisfying the following two conditions, and N is the number of data satisfying the following conditions.

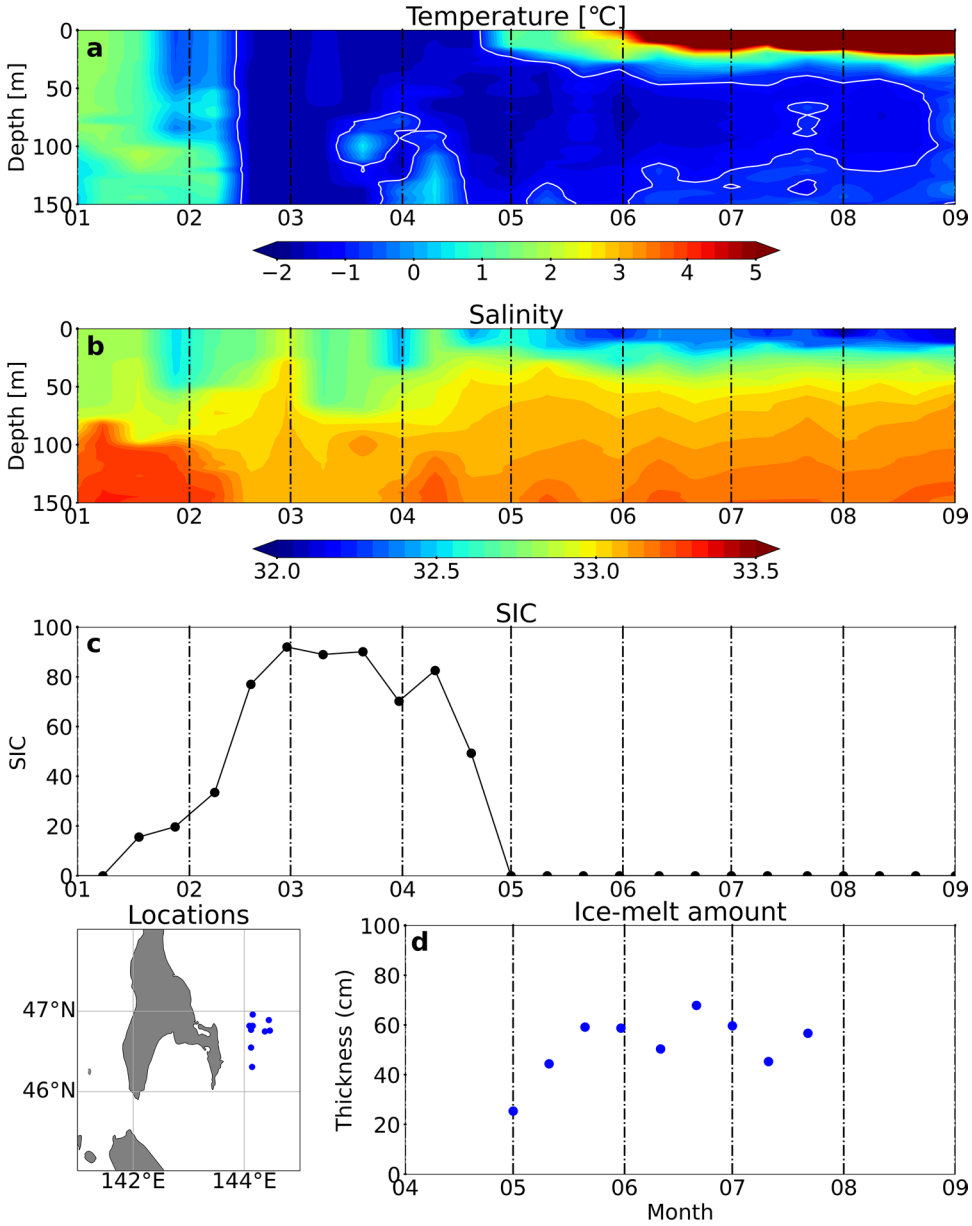

Fig. 4 Time series of **a** temperature, **b** salinity vertical profiles from the profiling float, **c** SIC averaged over the area within 25 km of the observational point, and **d** estimated ice-melt amount using each profile. The white contours in **a** indicate the temperature of − 1.0 °C. The small map on the lower left indicates the observational locations of the float

A. The profile is taken within 97 km (= L_r) from the grid center point.

B. The absolute value of Δh/h is less than 0.56 (= L_ϕ), where definitions of h and Δh are the same as those in Sect. 3.

The RMSE estimated in this way accounts for both the mapping error and the spatial variability of the ice-melt amount. It is noted that we excluded the grid points with less than 5 observational data points satisfying conditions of A and B in mapping of Fig. 6. Figure 7 shows the e_{95} divided by the ice-melt amount for each grid cell, expressed as a percentage. According to Fig. 7, the data reliability is relatively low in the eastern part of the Okhotsk Sea and the region around northern Sakhalin Island. The former is due to the small number of estimated data, and the latter is due to the large dispersion of the estimated values.

4.4 Interannual variability of sea-ice melt

One advantage of this study is that it provides sea ice information before the era of satellite observation using hydrographic data since the 1930s. This enables us to examine the longer term variability of sea ice. We confine the analysis area to the southern area (south of 48° N), where a relatively large number of ice-melt estimations was made (see Fig. 5). We used the gridded map of the ice-melt amount shown in Fig. 6 as the climatological mean. We used a relative rather than an absolute anomaly to minimize the bias caused by

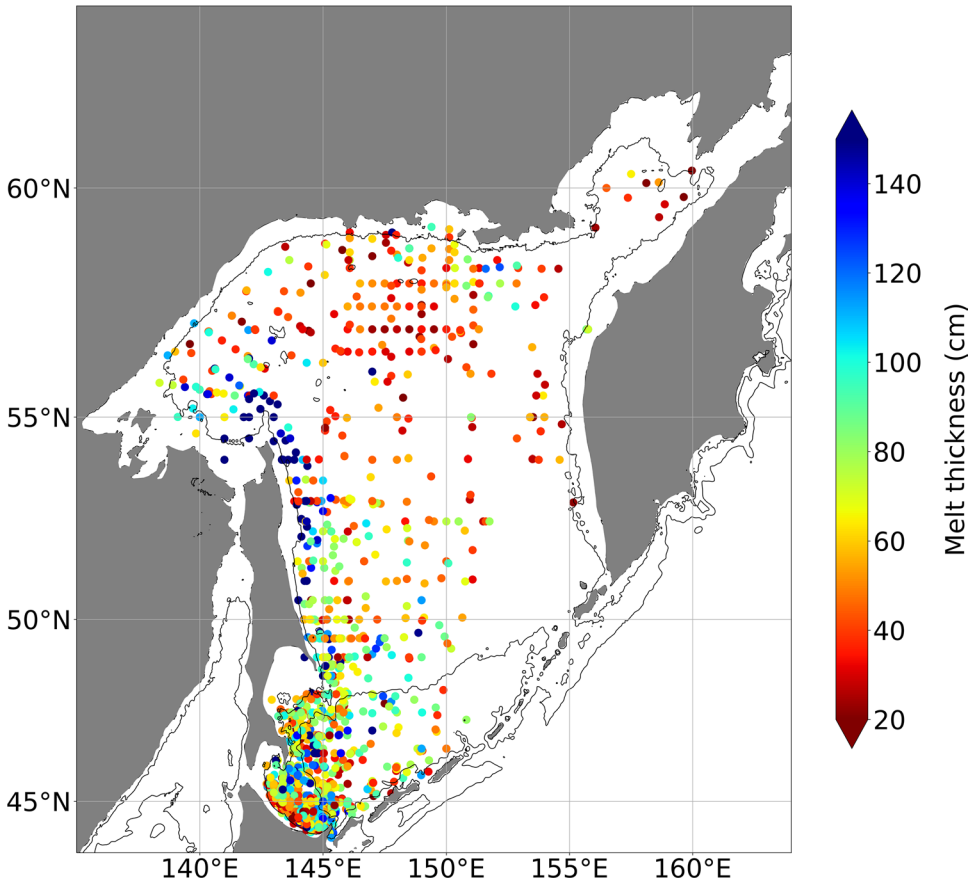

Fig. 5 Plots of sea-ice melt amounts estimated from all profiles in which the salinity deficit is detectable in the Sea of Okhotsk. The solid lines denote the bottom contours of 100 and 2000 m

the spatial difference in the ice-melt amount. For all the estimated data, we calculated the anomaly of ice-melt amount H_i from each profile relative to the climatological value H_{clm} in the grid cell in which the profile was taken. Then we calculated the relative anomaly ΔR_i in percent, defined as

$$\Delta R_i = \frac{H_i - H_{clm}}{H_{clm}} \times 100, \tag{5}$$

Next, all the calculated ΔR_i from individual profiles was averaged for each year and its average is defined as the yearly ice-melt anomaly ΔR_j. Further, we converted the yearly anomaly ΔR_j to the yearly ice-melt thickness H_j, using the average ice-melt thickness in the southern area H_{ave} (=71 cm), as follows:

$$H_j = H_{ave} + \left(\frac{\Delta R_j}{100} \times H_{ave} \right). \tag{6}$$

The black circles in Fig. 8a show the time series of yearly relative anomaly of ice-melt amount ΔR_j. As shown, the year-to-year variability and standard deviation for each year is very large, particularly before 1990. This is partly due to the small number of estimated data (see the estimated data number in Fig. 8c).

Figure 8c shows the time series of number of ice-melt estimated data with the data resolution indicated by color. Low-resolution data (orange bars) and high-resolution data (green bars) are defined by the vertical data point of <20 and of ≥ 20 within the upper 100 m, respectively. The average of the data point for low-resolution data is ~7 within the upper 100 m. Before 1990, all the estimated data are low-resolution data, while high-resolution data are dominant after 1990. To evaluate the error or bias in the ice-melt estimation arising from the low-resolution data, the following test was performed. First, original high-resolution data used for ice-melt estimation were discretized to 7 data points closest to the standard depths of 5, 10, 20, 30, 50, 75, 100 m within the surface 100 m. Then we estimated the ice melt amount with the same algorithm and calculation described in Sect. 3. When this test was applied to all the high-resolution data, the pseudo-discretized data show overestimation by ~15 cm in ice-melt thickness on average, compared to the estimation from the original data. This significant bias should not be ignored in the time series of ice-melt amount. Therefore, we also make the trend analysis, using only high-resolution data in the following analysis.

For the trend analysis, we calculated 5-year averages of ice-melt anomaly to increase reliability (blue circles and lines in Fig. 8a). Figure 8b shows the 5-year averages of ice-melt thickness converted from the 5-year relative anomalies. We first calculated the regression line of the 5-year averaged

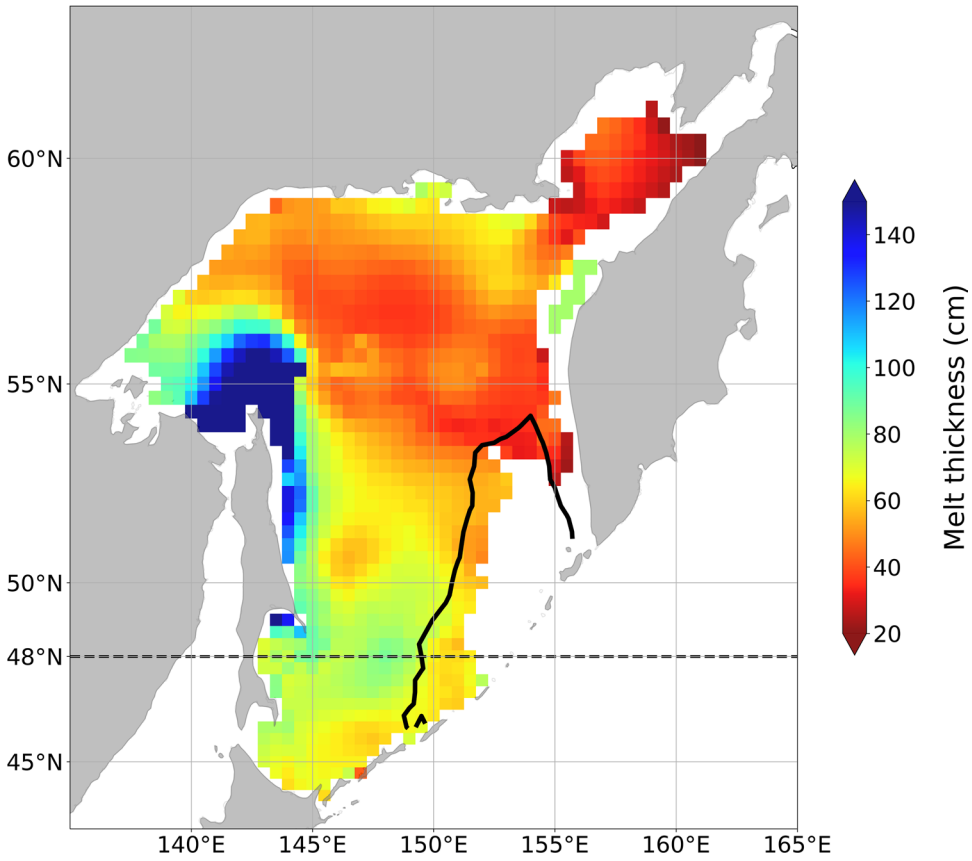

Fig. 6 Climatology map of the ice-melt amount in the Sea of Okhotsk, created by the shrinking and stretching constraint integrated scheme (Mensah and Ohshima 2023). The thick solid line indicates the boundary of the average sea-ice extent, defined in Sect. 3. The dotted lateral line indicates 48°N

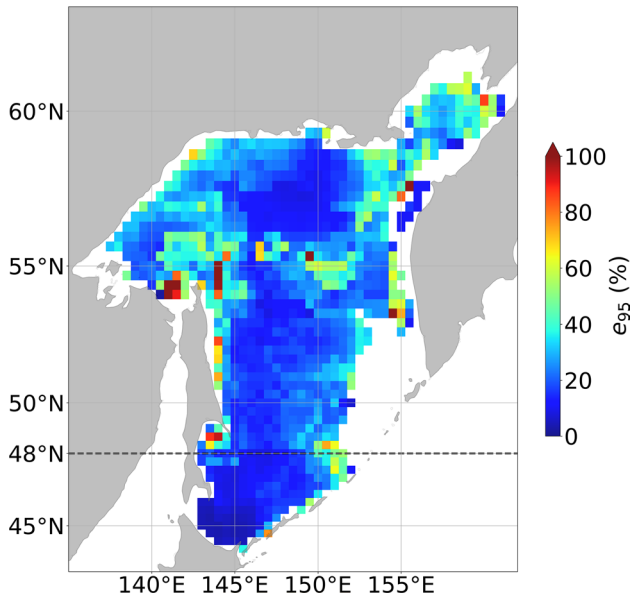

Fig. 7 Spatial distribution of error e_{95} divided by the ice-melt amount for each grid cell, expressed as a percentage

melt thicknesses from 1975 to present (orange line), when relatively large number of estimated data exists. The regression line demonstrates a prominent decreasing trend of –5.1 cm/decade for 1975–2023. Since this estimation may contain some bias due to the error/bias arising from the low-resolution for older data, we also calculated the regression line for 1990–2023, using only high-resolution data (green line). The resulting decreasing trend is –7.4 cm/decade. This implies that the ice-melt amount in the southern area of the Okhotsk Sea has decreased by ~ 30% over the past 30 years. The decrease in the ice-melt amount implies a decrease in ice transport to the south and a weakening of freshwater and heat transport by sea ice.

In contrast, there seems to be no significant trend for the period of 1930s–1970s, when the number of estimated data is small. We performed the independent-test among the averages of four periods of ice-melt thickness (pre–1955, 1955–1964, 1965–1974, 1975–1979) assuming Student's *t* distribution we found no significant differences for all pairs with a 99% confidence level. Continuous observations of sea ice started in the 1978/79 season by the satellite microwave radiometer. Our methodology can provide information on sea ice before the era of satellite observations. According to the above analysis, the ice-melt amount did not show a significant trend before the era of satellite observation. This suggests that the significant decline in sea ice did not occur in the Sea of Okhotsk during the 1930s–1970s, which could not be obtained by satellite observations.

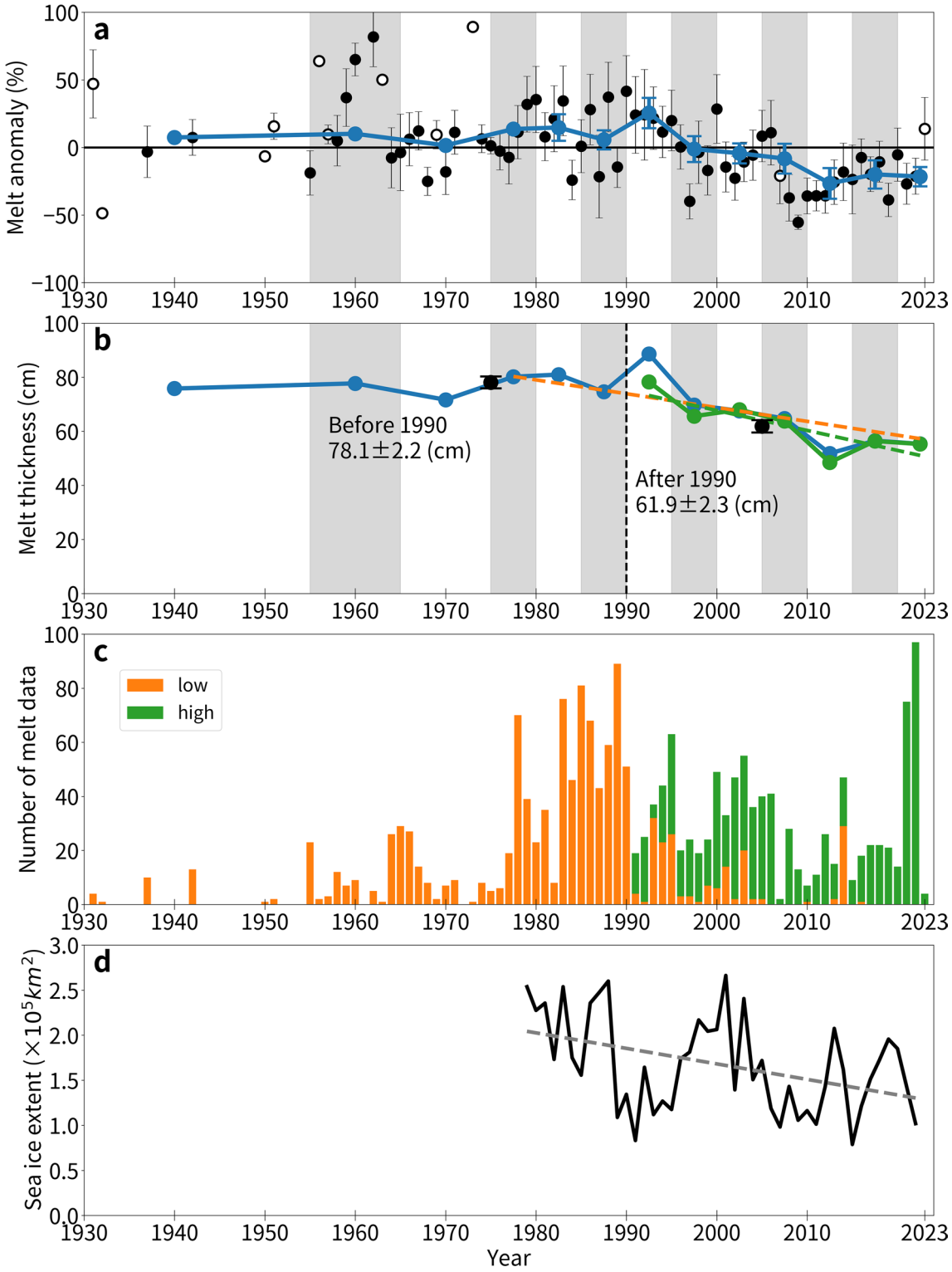

Most of sea ice and/or melting water in the shelf area in the southern part of the Okhotsk Sea comes from the north via the ESC and/or prevailing northerly wind (Kuga et al. 2023, 2024). To examine the influence of the advection from the north on the long-term variation, we compared the time series of ice-melt amount in the shelf area south of 48°N with that in the offshore deep area, where the effect of advection is relatively small (Fig. 9). The comparison shows that the shelf area exhibits a larger decreasing trend (–5.9 cm/decade) than the deeper area does (–3.5 cm/decade).

◂**Fig. 8** Time series of ice-melt amount and related information. **a** Yearly relative anomaly of ice-melt amount (black circles) with error bars representing the standard deviations of the anomaly for each year. Closed circles represent yearly anomalies for years with a data number of ≥ 5, and open circles represent yearly anomalies for years with a data number of < 5. Blue thick lines and circles indicate 5-year averages of relative anomalies after 1975 with error bars representing 95% confidence intervals. Before 1975, when the number of the estimated data is small, the averages were calculated for 1930–1954, 1955–1964, 1965–1974. **b** Averages of ice-melt thickness (blue and green lines) converted from the averages of all relative anomalies shown in **a** and for only from the high-resolution data during 1990–2023, respectively. The orange and green lines represent the regression lines for all the data during 1975–2023 and for only from the high-resolution data during 1990–2023, respectively. The black circles represent the averages of ice-melt thickness for two periods, before and after 1990, with error bars representing 95% confidence intervals for each average. **c** Number of data that can estimate ice-melt amount for each year. Orange bars indicate the low-resolution data defined by the vertical data point of < 20 within the upper 100 m, and green bars indicate the high-resolution data defined by the vertical data point of ≥ 20 within the upper 100 m. **d** Yearly variation of the maximum sea-ice extent south of 48° N, calculated from the SIC data, with the regression line indicated by the gray dashed line (color figure online)

5 Analysis of the salinity change in spring

Aside from estimating the ice-melt amount from the salinity deficit, we also analyzed the salinity change in the southern area of the Okhotsk Sea (south of 48°N), by dividing it into two periods before 1990 and after 1990. The gridded dataset was created from all observational data in April and May based on the mapping methodology of Mensah and Ohshima (2023). The locations of the salinity data points used in the gridded dataset are shown in supplementary information (Figure S2). We also obtained gridded data on buoyancy frequency N^2 in April and May to examine the stratification change. N^2 is represented by

$$N^2 = \frac{g}{\rho}\frac{d\rho}{dz}, \tag{7}$$

where g is the acceleration of gravity, z is the depth, and ρ is the density.

The salinity for the two periods before and after 1990 and their differences are shown for depths of 0, 20, 50, and 100 m (Fig. 10). The salinity has increased at 0 and 20 m depths while it decreased at 100 m in most areas. The red line in Fig. 11 shows the vertical profile of the difference in salinity between the two periods averaged south of 48°N. Between the two periods, salinity increased in the upper 50 m layer while decreased in the layer below 50 m. Ohshima et al. (2014) suggested freshening at 50−500 m layer over most areas in the Sea of Okhotsk, even in the southern part. The buoyancy frequency at 20 m for the two periods (Fig. 12) clearly shows that the stratification has been weakened in most areas. Increased salinity in the upper layer and decreased salinity in the lower layer have led to weakening of the stratification in the upper 100 m layer (blue line in Fig. 11).

We converted the salinity increase in the upper 50 m layer between the two periods to the decrease in freshwater supply. Conservation of salinity for the water column with the thickness of H between the two periods represents

$$S_0 \times \left(H - x_F\right) = H \times \left(S_0 + \Delta S_a\right), \tag{8}$$

where S_0 is the averaged salinity in the former period (before 1990), ΔS_a is the averaged salinity difference between the two periods (after 1990 minus before 1990), x_F is the freshwater thickness corresponding to the salinity difference, and we assume $H \gg x_F$.

The freshwater thickness x_F is given by

$$x_F = \frac{-H \times \Delta S_a}{S_0}, \tag{9}$$

If we assume that all the salinity decrease (freshening) is caused by sea-ice melt, the corresponding ice-melt amount in thickness th_i is calculated to be

$$th_i = \frac{S_0}{S_0 - S_i} \times \frac{\rho_w}{\rho_i} \times x_F, \tag{10}$$

where sea ice and sea water densities are assumed to be $\rho_i = 900(kg/m^3)$ and $\rho_w = 1025(kg/m^3)$, respectively. The salinity of sea ice S_i is set to 4.6. S_w is set to 32.6, the average of the upper 50 m layer.

Figure 13 shows the horizontal distribution of the change in salt content in the upper layer between the two periods before and after 1990, converted to the ice-melt amount in thickness. Although the absolute value of the ice-melt amount cannot be obtained by this salinity dataset, a change in the ice-melt amount can be inferred. Most of the southern area of the Okhotsk Sea exhibits an ice-melt decrease, except for the nearshore area off the Hokkaido coast which is largely affected by the Soya Warm Current. The decrease in freshwater supply and ice-melt amount is 10.9 cm and 14.1 cm, respectively, averaged over the region south of 48°N by excluding areas shallower than 150 m to remove the effects of the Soya Warm Current. The two independent methods described in this section and Sect. 4.4 show consistent results of the decrease in sea-ice melting. These results support the method for estimating the amount of ice melting and the change of ice-melt amount. To check the sensitivity to the selected periods, we also created a salinity dataset for two periods before and after 2000 and calculated the change in freshwater supply and ice-melt amount similarly. The decreases in freshwater supply and ice-melt amount are 7.7 cm and 10.2 cm, respectively. According to Fig. 13, the area of 46–47°N and east of 146°E, and the area around

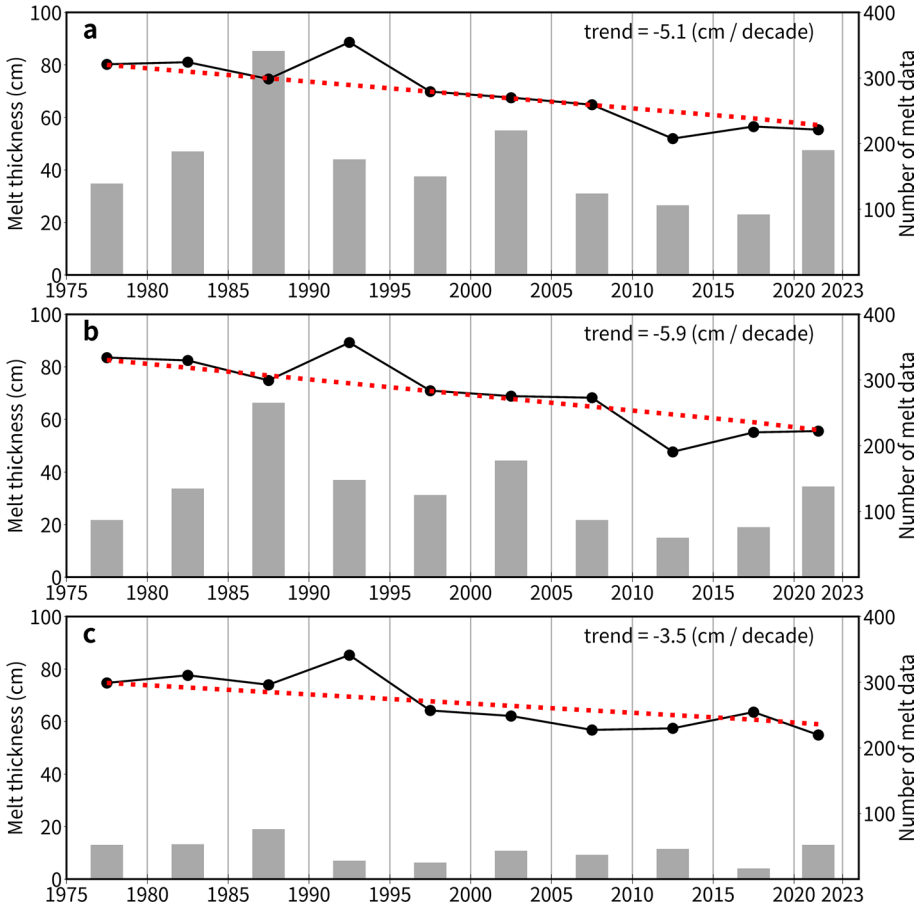

Fig. 9 a Time series of ice-melt amount averaged in 5 years in the southern part of Okhotsk Sea, separated into b coastal sharrow area of < 1500 m in depth, c offshore deep area of ≥ 1500 m in depth. Gray bars represent number of data that can estimate the ice melt for each year. Red dotted line shows the regression lines of 5–year averages (color figure online)

the Shiretoko Peninsula show particularly large decreases in sea-ice melt. According to the monthly maps of hydrography by Mensah et al. (2019), these areas correspond to areas that pool the light surface water after spring.

In this study, we have revealed that the ice-melt amount has been decreasing in the southern area of the Okhotsk Sea, which is an ice-melt-dominant area. In contrast, in the northwestern area of the sea, an ice-production-dominant area, Ohshima et al. (2014) revealed a significant freshening and decrease in Dense Shelf Water over the past 40 years and suggested the weakening of salt and heat redistribution by sea-ice decline. Combined with that study, the decrease in ice production over the past 40 years has led to a decrease in sea ice transport to the south and, accordingly, a decrease in freshwater and negative heat transport by ice melting. These changes may affect the regional climate. Further, they potentially affect biological production through the weakening of stratification by the decreased ice melt and decreased transport of materials such as iron with sea ice.

6 Discussion

The amount of sea ice melt is estimated to be 71 cm in thickness on average in the southern area of the Okhotsk Sea. After the ice melts, meltwater would be advected or diffused by the ocean current and wind. Advection and diffusion of the meltwater cannot be ignored in the Kuril Basin, where the activity of mesoscale eddies is particularly strong (Bulatov et al. 1999). If the meltwater is diffused towards the open water area, the ice melt amount tends to be thinner than the ice thickness before melting. However, evaluating the effects of diffusion and advection is difficult only from observations. Furthermore, our conversion of the ice-melt amount into ice thickness implicitly assumes SIC of 100%. In reality, the SIC is slightly lower than 100% in sea-ice-covered areas.

In the southern area of the Okhotsk Sea, there have been several direct observations of sea-ice thickness with

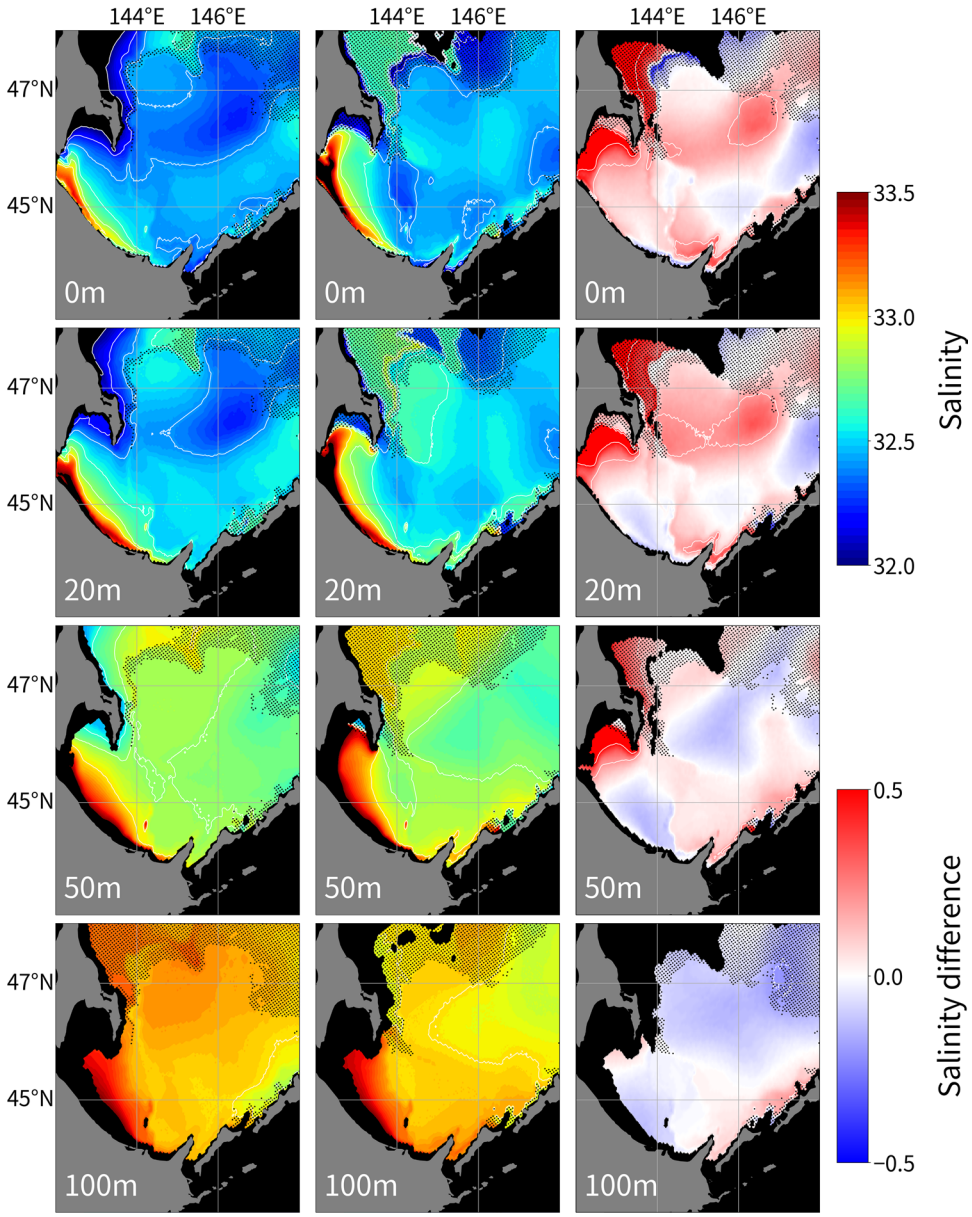

Fig. 10 Horizontal distributions of salinity at depths of 0, 20, 50, and 100 m in the southern area of the Okhotsk Sea for two periods, before 1990 (left panels), after 1990 (center panels), and their difference (right panels). The grid cell with data number of < 10 are indicated by the black dots

various methods off the coast of Hokkaido. Observations with a moored ice-profiling sonar revealed an average ice thickness of 71 cm in 1999–2001 off the coast of Hokkaido (Fukamachi et al. 2003, 2006). Observations with ship-borne electromagnetic inductive showed an average ice thickness of 61 cm in 2004 and 75 cm in 2005 (Uto et al. 2006). Visual observations onboard the icebreaker Soya using the ASPeCt protocol conducted during 1996–2020 showed an average ice thickness of 64 ± 38 cm (Toyota et al. 2022). These values correspond well to the melt-ice thickness of 62 cm averaged over the southern area of the Okhotsk Sea during 1990–2023 (Fig. 8b).

According to Fig. 6, the coastal area around northern Sakhalin Island shows the largest amount of ice melt, 120–150 cm, which is qualitatively consistent with the ice thickness distribution obtained from the satellite observations (Nihashi et al. 2018). The mooring observation off the coast of Sakhalin at 53° N (Fukamachi et al. 2009) showed an average ice thickness of 120 cm, which is comparable to our estimated ice melt thickness. However, it is noted that the salinity deficit in the surface layer around this region may contain freshwater from the Amur River. Thus, the estimated ice melt is probably overestimated, although we cannot extract the component of the Amur discharge only from the temperature and salinity profile. Observations of $\delta^{18}O$ will be required for evaluation of the Amur discharge on the salinity deficit.

Instead, we identify the area where the salinity deficit is affected by the Amur discharge. The river water freezes during winter, and the discharge from the river increases

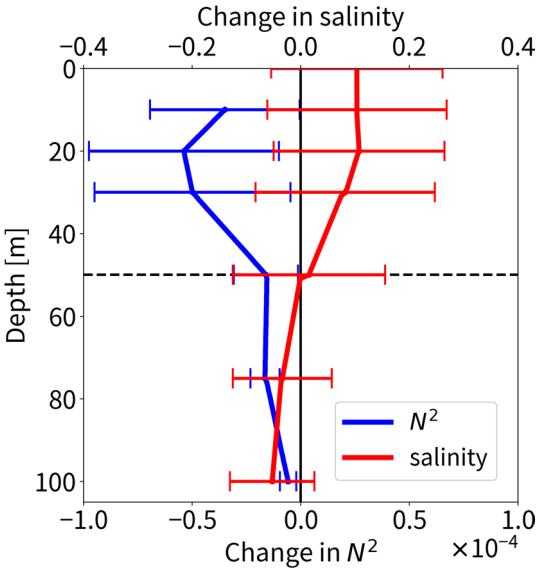

Fig. 11 Vertical profiles of the difference in salinity (red line) and buoyancy frequency N^2 (blue line) between the two periods, averaged over the southern area of the Okhotsk Sea (south of 48°N). Error bars indicate standard deviations (color figure online)

dramatically after May (Ogi et al. 2001). Freshwater from this discharge is transported southward by the nearshore branch of the ESC. Mizuta et al. (2003) estimated that the southern limit of the Amur water reaches to 53°N in July, based on the observed current speed and salinity. The profiles used for ice-melt estimation off the Sakhalin coast were mostly taken in June/July, 1–2 months after the discharge explosion. Thus, there is a high probability that the estimated ice-melt amount north of 53°N is overestimated. In the southern area (south of 48° N) we focused on, we mostly used data before July to estimate the ice melt amount. Hence, the effect of the Amur water on estimation of ice-melt amount is negligible in the southern area.

In the coastal area around northern Sakhalin north of 53°N, surface low salinity water can be advected by ~ 300 km to the south, referring the advection length estimated by Mizuta et al. (2003). Thus, the estimated ice-melt amount in this region possibly reflects the information in the upstream areas. While, in the southern Sakhalin coast, the mean current is small (less than 5 cm/s) during May–July, according to the mooring observation and model results (Ohshima and Simizu 2008). Also in the western part of the Kuril Basin, the mean current is small (less than 5 cm/s) in spring (Mensah et al. 2019). Therefore, we consider that effects of the advection on the ice-melt amount is not critical in the southern area.

In addition to river discharge, precipitation to the ocean in spring, and snow cover on sea ice in winter may contribute to the salinity deficit, although the melting of sea ice is the major contributor to the salinity deficit. Here we evaluated the effects of precipitation and snow cover. According to the European Centre for Medium-Range Weather Forecasts (ECMWF) ERA5 data, precipitation–evaporation in spring (April–June) is integrated to be ~ 6.4 cm for the averaged elapsed time of 47 days after the ice melt, which is less than 10% of the-ice melt amount. Regarding snow cover, the mass fraction of snow to the total sea ice occupies only ~ 1–2% (Toyota et al. 2007), corresponding to an ice-melt amount of ~ 1 cm in thickness. These evaluations suggest that precipitation and snow cover do not significantly affect the estimation of the ice-melt amount (less than 10%).

The prevailing northerly wind induces an onshore Ekman transport and the subsequent piling-up of surface water off the Sakhalin and Hokkaido coast, strongly in winter and weakly in spring (Mizuta et al. 2004; Mensah et al. 2019). Thus, the surface freshened layer by sea-ice melt is possibly affected by this piling-up. However, the total freshening (salinity deficit) does not change, and the estimation of the total ice-melt amount would not be changed.

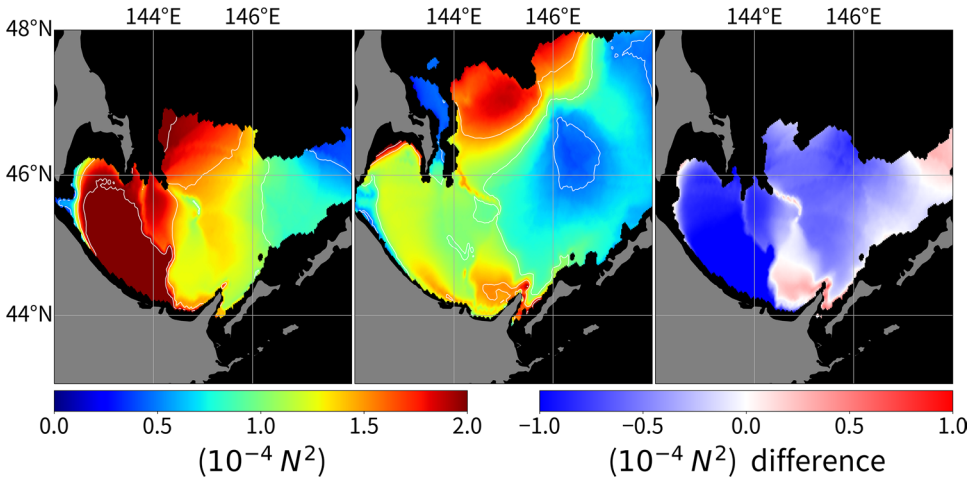

Fig. 12 Horizontal distributions of the buoyancy frequency N^2 at 20 m in the southern area of the Okhotsk Sea for the two periods before 1990 (left panel), after 1990 (center), and their difference (right)

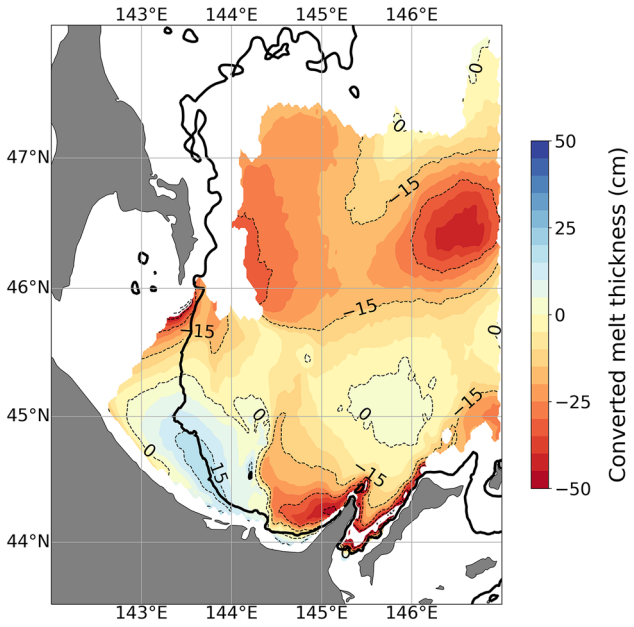

Fig. 13 The salinity changes in the upper 50 m layer between the two periods before and after 1990, converted to the melt amount of sea ice in thickness. Black lines indicate the bottom contours of 150 m (color figure online)

One drawback of our study is the uneven estimation of the ice-melt amount both spatially and temporally. Thus, it is difficult to discuss the year-to-year variation in the ice-melt amount using only our estimated data. One way to evaluate the yearly variation of the ice-melt amount is through the combined use of satellite passive microwave data, which has been accumulated for nearly half a century since 1978. Tamura et al. (2011) and Nihashi et al. (2012) tried to estimate the ice-melt amount using satellite microwave data in the Southern Ocean and Sea of Okhotsk, respectively. However, their estimations include several ad-hoc assumptions, such as that the melted ice thickness is constant over the entire area, partly because there were no validation data for the ice-melt amount. This study would provide useful validation data for the ice-melt amount. One challenge in the future is to develop a satellite microwave algorithm for estimating the ice-melt amount, using our estimated data as validation data.

This study revealed that the ice-melt amount in the southern area of the Okhotsk Sea has decreased by ~ 30% over the past 30 years. Here, we briefly discuss the cause and effect of this result in terms of its relationship with global warming, as schematically shown in Fig. 14. The upwind area of the Okhotsk Sea is highly sensitive to global warming, and the increased rate of air temperature in this area in the fall and winter is three times larger than the global average (e.g., Nakanowatari et al. 2007). This warming has resulted in a decrease in sea ice production in the coastal polynyas (Kashiwase et al. 2014). Then, the salinity of Dense Shelf Water has decreased, leading to the weakening of intermediate overturning (Ohshima et al. 2014; Mensah and Ohshima 2021). Owing to the decrease in ice production, the amount of ice advected and melted in the south has decreased. Hence, the freshwater input to the ocean surface has decreased, and spring stratification has been weakened. This might affect biological production in the Sea of Okhotsk on a half-century scale because the spring intensification of surface stratification is one of the key factors in the spring phytoplankton bloom in the Sea of Okhotsk (Sorokin and Sorokin 1999).

Because spring hydrographic data have been accumulated in the southern area of the Okhotsk Sea since the 1930s (Fig. 8c), our study may provide the information on sea ice before the era of satellite observations. According to our analysis, the ice-melt amount did not show a significant trend during the 1930s–1970s, although the significance is not high because of sparse data. This result suggests that a decline in sea ice did not occur in the Sea of Okhotsk during the 1930s–1970s. As such, our methodology possibly extracts the information on sea ice before the era of satellite observations.

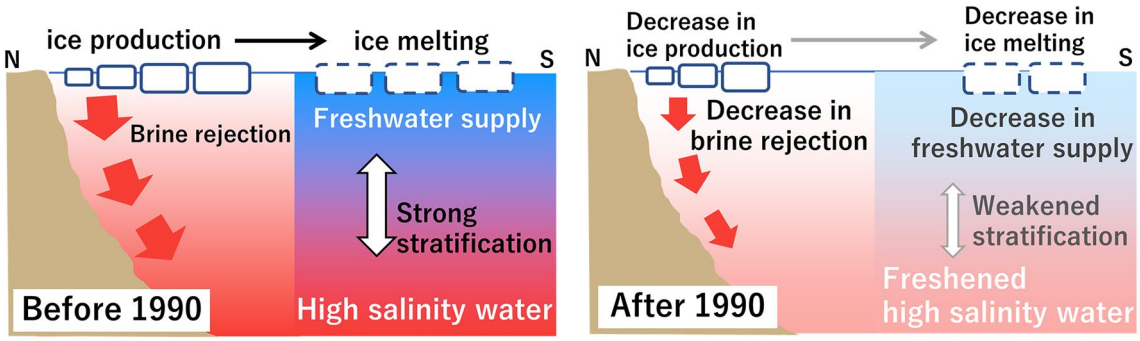

Fig. 14 Schematic diagram of the redistribution of freshwater/salt by sea ice and its changes in the Sea of Okhotsk

Appendix

Here, we describe the details of the algorithm to extract appropriate profiles to estimate the ice-melt amount and identify the deepest depth affected by sea-ice melt. In addition to the vertical point data profiles of temperature and salinity, their gradients calculated from the vertically consecutive two-point data were also used in the algorithm. First, we extracted profiles of Type A, in which the meltwater layer is clearly separated from the underlying WW layer (Fig. 2a). Primarily, the temperature is read from the surface to deeper depths, defined as the positive direction. If a large gradient of >0.1 °C/m is found between 10 and 80 m in depth (detection of warming), further reading is continued to search for a positive or negative gradient of <0.01 °C /m with a temperature of <-1.0 °C (search for a uniform WW layer). If such a profile can be found, its shallowest depth is set to D_A (tentative top of the WW layer), and the temperature and salinity at D_A are defined as T_A and S_A, respectively. Then further reading is continued to check whether the temperature at the depth of D_A+50 m is lower than $T_A+0.7$ °C (check of uniformity). If all these conditions are satisfied, those profiles are tentatively categorized as Type A in terms of temperature profile. Next, we checked the salinity profiles for the upper layer above D_A. If a salinity gradient of >0.02 psu/m exists in the layer and the difference between S_A and the salinity averaged over the upper D_A layer is more than 0.1 psu (detection of freshening), that profile is finally categorized as Type A, and D_A is regarded as the deepest depth affected by sea-ice melt.

Immediately after the sea ice melts, the profile should be Type A. As time passes, the vertically uniform WW layer is eroded by mixing both from the top and bottom and the temperature minimum occurs, as typically shown in Fig. 2b. If this minimum temperature (T_{min}) is sufficiently close to the freezing temperature and T_{min} depth is defined as D_B, it is likely that only the surface layer above D_B is affected by the ice melting and the salinity at D_B keeps the WW salinity. Such profiles are categorized as Type B with the following conditions being satisfied: the temperature minimum T_{min} is less than -1.0 °C and the temperature at the depth of D_B+30 m is less than $T_{min}+0.3$ °C (detection of remnants of WW). Regarding the salinity profile for Type B, we applied the same conditions as those for Type A. The values of z_0 and Sz_0 for calculating the ice-melt amount in Eq. (1) are D_A and S_A for Type A, and D_B and S_B for Type B, respectively. It is noted that we excluded the profiles whose uppermost data point was deeper than 10 m as the crucial near-surface data are missing from such profiles.

Supplementary Information The online version contains supplementary material available at https://doi.org/10.1007/s10872-024-00721-z.

Acknowledgements The authors express their gratitude to Kyoko Kitagawa for her support. The authors are deeply indebted to Wakkanai Fisheries Research Institute of Hokkaido Research Organization for providing the hydrographic data. We thank Yoko Mitani (Kyoto University) for obtaining the biologging data. The figures were produced with some Python packages. We appreciate helpful comments by two anonymous reviewers, which contributed to improve this manuscript. This work was supported by Grants-in-Aids for Scientific Research (20H05707, 22K14094, 21H05056) and the Arctic Challenge for Sustainability II project from the Ministry of Education, Culture, Sports, Science and Technology in Japan. This work was also supported by a research fund for Global Change Observation Mission Water 1 (GCOM-W1) of the Japan Aerospace Exploration Agency (JAXA) (PI No. ER2GWF404 and ER3AMF424).

Data availability Historical CTD data were downloaded as part of the World Ocean Database 2018, a National Centers for Environmental Information standard product. The profiling float data in the Sea of Okhotsk from the joint University of Washington—Hokkaido University project will be released in 2024.

References

Andreev A, Pipko I (2022) Water circulation, temperature, salinity, and pCO2 distribution in the surface layer of the east kamchatka current. J Mar Sci Eng 10(11):1787. https://doi.org/10.3390/jmse10111787

Boyer TP, Baranova OK, Coleman C, Garcia HE, Grodsky A, Locarnini RA, Mishonov AV, Paver CR, Reagan JR, Seidov D, Smolyar IV, Weathers KW, Zweng MM (2018) World Ocean Database

Bulatov NV, Kurennaya LA, Muktepavel LS, Aleksanina MG, Gerbek EE (1999) Eddy water structure in the southern Okhotsk Sea and its seasonal variability (results of satellite monitoring). Oceanology 39:29–37

Comiso JC (1995) SSM/I Sea Ice Concentrations Using the Bootstrap Algorithm. NASA Reference Publication 1380

Fukamachi Y, Mizuta G, Ohshima KI, Melling H, Fissel D, Wakatsuchi M (2003) Variability of sea-ice draft off Hokkaido in the Sea of Okhotsk revealed by a moored ice-profiling sonar in winter of 1999. Geophys Res Lett 30:29–32. https://doi.org/10.1029/2002GL016197

Fukamachi Y, Mizuta G, Ohshima KI, Toyota T, Kimura N, Wakatsuchi M (2006) Sea ice thickness in the southwestern Sea of Okhotsk revealed by a moored ice-profiling sonar. J Geophys Res 111:1–12. https://doi.org/10.1029/2005JC003327

Fukamachi Y, Shirasawa K, Polomoshnov AM, Ohshima KI, Kalinin E, Nihashi S, Melling H, Mizuta G, Wakatsuchi M (2009) Direct observations of sea-ice thickness and brine rejection off

Sakhalin in the Sea of Okhotsk. Cont Shelf Res 29:1541–1548. https://doi.org/10.1016/j.csr.2009.04.005
Kanna N, Toyota T, Nishioka J (2014) Iron and macro-nutrient concentrations in sea ice and their impact on the nutritional status of surface waters in the southern Okhotsk Sea. Prog Oceanogr 126:44–57. https://doi.org/10.1016/j.pocean.2014.04.012
Kanna N, Sibano Y, Toyota T, Nishioka J (2018) Winter iron supply processes fueling spring phytoplankton growth in a sub-polar marginal sea, the Sea of Okhotsk: importance of sea ice and the East Sakhalin Current. Mar Chem 206:109–120. https://doi.org/10.1016/j.marchem.2018.08.006
Kashiwase H, Ohshima KI, Nihashi S (2014) Long-term variation in sea ice production and its relation to the intermediate water in the Sea of Okhotsk. Prog Oceanogr 126:21–32. https://doi.org/10.1016/j.pocean.2014.05.004
Kida S, Qiu B (2013) An exchange flow between the Okhotsk Sea and the North Pacific driven by the East Kamchatka Current. J Geophys Res. https://doi.org/10.1002/2013JC009464
Kimura N, Wakatsuchi M (2004) Increase and decrease of sea ice area in the Sea of Okhotsk: Ice production in coastal polynyas and dynamic thickening in convergence zones. J Geophys Res 109:JC001903. https://doi.org/10.1029/2003JC001901
Kishi S, Ohshima KI, Nishioka J, Isshiki N, Nihashi S, Riser SC (2021) The prominent spring bloom and its relation to sea-ice melt in the Sea of Okhotsk, revealed by profiling floats. Geophys Res Lett 48:1–9. https://doi.org/10.1029/2020GL091394
Kuga M, Ohshima KI, Kimura N (2023) Particle-tracking experiments of coastal-origin sea ice that could induce high biological productivity in the Sea of Okhotsk. J Oceanogr 79:145–159. https://doi.org/10.1007/s10872-022-00670-5
Kuga M, Ohshima KI, Kishi S, Kimura N, Toyota T, Nishioka J (2024) Backward-tracking simulations of sea ice in the Sea of Okhotsk toward understanding of material transport through sea ice. J Oceanogr 80:59–70. https://doi.org/10.1007/s10872-023-00706-4
Martinson DG, Iannuzzi RA (1998) Antarctic ocean-ice interaction: implications from ocean bulk property distributions in the Weddell gyre. Antarct Res Ser 74:243–271
Mensah V, Ohshima KI (2021) Weakened overturning and tide control the properties of Oyashio Intermediate Water, a key water mass in the North Pacific. Sci Rep 11:1–15. https://doi.org/10.1038/s41598-021-93901-6
Mensah V, Ohshima KI (2023) A mapping methodology adapted to all polar and subpolar oceans with a stretching/shrinking constraint. J Atmos Oceanic Technol. https://doi.org/10.1175/JTECH-D-22-0143.1
Mensah V, Ohshima KI, Nakanowatari T, Riser SC (2019) Seasonal changes of water mass, circulation and dynamic response in the Kuril Basin of the Sea of Okhotsk. Deep Sea Res I 144:115–131. https://doi.org/10.1016/j.dsr.2019.01.012
Mizuta G, Fukamachi Y, Ohshima KI, Wakatsuchi M (2003) Structure and seasonal variability of the east sakhalin current. J Phys Oceanogr 33:2430–2445. https://doi.org/10.1175/1520-0485(2003)033%3c2430:SASVOT%3e2.0.CO;2
Mizuta G, Ohshima KI, Fukamachi Y, Itoh M, Wakatsuchi M (2004) Winter mixed layer and its yearly variability under sea ice in the southwestern part of the Sea of Okhotsk. Cont Shelf Res 24:643–657. https://doi.org/10.1016/j.csr.2004.01.006
Nakanowatari T, Ohshima KI, Wakatsuchi M (2007) Warming and oxygen decrease of intermediate water in the northwestern North Pacific, originating from the Sea of Okhotsk, 1955–2004. Geophys Res Lett 34:L04602. https://doi.org/10.1029/2006GL028243
Nakanowatari T, Ohshima KI, Nagai S (2010) What determines the maximum sea ice extent in the Sea of Okhotsk?: Importance of ocean thermal condition from the Pacific. J Geophys Res 115:C12031. https://doi.org/10.1029/2009JC006070
Nakanowatari T, Ohshima KI, Mensah V, Mitani Y, Hattori K, Kobayashi M, Roquet F, Sakurai Y, Mitsudera H, Wakatsuchi M (2017) Hydrographic observations by instrumented marine mammals in the Sea of Okhotsk. Polar Sci 13:56–65. https://doi.org/10.1016/j.polar.2017.06.001
Nakata K, Ohshima KI (2022) Mapping of active frazil and sea ice production in the Northern Hemisphere, with comparison to the Southern Hemisphere. J Geophys Res 127:e2022JC018553. https://doi.org/10.1029/2022JC018553
Nihashi S, Ohshima KI, Tamura T, Fukamachi Y, Saitoh SI (2009) Thickness and production of sea ice in the Okhotsk Sea coastal polynyas from AMSR-E. J Geophys Res 114:C10025. https://doi.org/10.1029/2008JC005222
Nihashi S, Ohshima KI, Nakasato H (2011) Sea-ice retreat in the Sea of Okhotsk and the ice-ocean albedo feedback effect on it. J Oceanogr 67:551–562. https://doi.org/10.1007/s10872-011-0056-x
Nihashi S, Ohshima KI, Kimura N (2012) Creation of a heat and salt flux dataset associated with sea ice production and melting in the Sea of Okhotsk. J Clim 25:2261–2278. https://doi.org/10.1175/JCLI-D-11-00022.1
Nihashi S, Kurtz NT, Markus T, Ohshima KI, Tateyama K, Toyota T (2018) Estimation of sea-ice thickness and volume in the Sea of Okhotsk based on ICESat data. Annals Glaciol 59:101–111. https://doi.org/10.1017/aog.2018.8
Ogi M, Tachibana Y, Nishio F, Danchenkov MA (2001) Dose the fresh water supply from the Amur river flowing into the Sea of Okhotsk affect sea ice formation? J Meteor Soc Japan 79:123–129. https://doi.org/10.2151/jmsj.79.123
Ohshima KI, Simizu D (2008) Particle tracking experiments on a model of the Okhotsk Sea: toward oil spill simulation. J Oceanogr 64:103–114. https://doi.org/10.1007/s10872-008-0008-2
Ohshima KI, Mizuta G, Itoh M, Fukamachi Y, Watanabe T, Nabae Y, Suehiro K, Wakatsuch M (2001) Winter oceanographic conditions in the southwestern part of the Okhotsk Sea and their relation to sea ice. J Oceanogr 57:451–460. https://doi.org/10.1023/A:1021225303621
Ohshima KI, Wakatsuchi M, Fukamachi Y, Mizuta G (2002) Near-surface circulation and tidal currents of the Okhotsk Sea observed with satellite-tracked drifters. J Geophys Res 107:3195. https://doi.org/10.1029/2001JC001005
Ohshima KI, Watanabe T, Nihashi S (2003) Surface heat budget of the Sea of Okhotsk during 1987–2001 and the role of sea ice on it. J Meteorol Soc Japan 81:653–677. https://doi.org/10.2151/jmsj.81.653
Ohshima KI, Simizu D, Itoh M, Mizuta G, Fukamachi Y, Riser SC, Wakatsuchi M (2004) Sverdrup balance and the cyclonic gyre in the Sea of Okhotsk. J Phys Oceanogr 34:513–525. https://doi.org/10.1175/1520-0485(2004)034%3c0513:SBATCG%3e2.0.CO;2
Ohshima KI, Riser SC, Wakatsuchi M (2005) Mixed layer evolution in the Sea of Okhotsk observed with profiling floats and its relation to sea ice formation. Geophys Res Lett 32:L06607. https://doi.org/10.1029/2004GL021823
Ohshima KI, Nakanowatari T, Riser SC, Wakatsuchi M (2010) Seasonal variation in the in- and outflow of the Okhotsk Sea with the North Pacific. Deep Sea Res II 57:1247–1256. https://doi.org/10.1016/j.dsr2.2009.12.012
Ohshima KI, Nakanowatari T, Riser SC, Volkov Y, Wakatsuchi M (2014) Freshening and dense shelf water reduction in the Okhotsk sea linked with sea ice decline. Prog Oceanogr 126:71–79. https://doi.org/10.1016/j.pocean.2014.04.020
Ohshima KI, Nihashi S, Iwamoto K (2016) Global view of sea-ice production in polynyas and its linkage to dense/bottom water formation. Geosci Lett 3:13. https://doi.org/10.1186/s40562-016-0045-4
Ohshima KI, Simizu D, Ebuchi N, Morishima S, Kashiwase H (2017) Volume, heat, and salt transports through the soya strait and their

seasonal and interannual variations. J Phys Oceanogr 47:999–1019. https://doi.org/10.1175/JPO-D-16-0210.1

Prants SV, Andreev AG, Budyansky MV, Uleysky YM (2015) Impact of the Alaskan Stream flow on surface water dynamics, temperature, ice extent, plankton biomass, and walleye pollock stocks in the eastern Okhotsk Sea. J Mar Sys 151:47–56. https://doi.org/10.1016/j.jmarsys.2015.07.001

Shcherbina AY, Talley LD, Rudnick DL (2003) Direct observations of North Pacific ventilation: brine rejection in the Okhotsk Sea. Science 302:1952–1955. https://doi.org/10.1126/science.1088692

Shimada K, Aoki S, Ohshima KI (2017) Creation of a gridded dataset for the Southern Ocean with a topographic constraint scheme. J Atmos Oceanic Technol 34:511–532. https://doi.org/10.1175/JTECH-D-16-0075.1

Simizu D, Ohshima KI (2006) A model simulation on the circulation in the Sea of Okhotsk and the East Sakhalin Current. J Geophys Res 111:C05016. https://doi.org/10.1029/2005JC002980

Simizu D, Ohshima KI, Ono J, Fukamachi Y, Mizuta G (2014) What drives the southward drift of sea ice in the Sea of Okhotsk? Prog Oceanogr 126:33–43. https://doi.org/10.1016/j.pocean.2014.05.013

Sorokin YI, Sorokin PY (1999) Production in the sea of Okhotsk. J Plankton Res 21:201–230. https://doi.org/10.1093/plankt/21.2.201

Talley LD (1991) An Okhotsk Sea water anomaly: implications for ventilation in the North Pacific. Deep Sea Res Part A 38:S171–S190. https://doi.org/10.1016/s0198-0149(12)80009-4

Tamura T, Ohshima KI, Nihashi S, Hasumi H (2011) Estimation of surface heat/salt fluxes associated with sea ice growth/melt in the Southern Ocean. SOLA 7:17–20. https://doi.org/10.2151/sola.2011-005

Toyota T, Takatsuji S, Tateyama K, Naoki K, Ohshima KI (2007) Properties of sea ice and overlying snow in the Southern Sea of Okhotsk. J Oceanogr 63:393–411. https://doi.org/10.1007/s10872-007-0037-2

Toyota T, Kimura N, Nishioka J, Ito M, Nomura D, Mitsudera H (2022) The Interannual Variability of Sea Ice Area, Thickness, and Volume in the Southern Sea of Okhotsk and Its Likely Factors. J Geophys Res 127:e2022JC019069. https://doi.org/10.1029/2022JC019069

Uto S, Toyota T, Shimoda H, Tateyama K, Shirasawa K (2006) Shipborne electromagnetic induction sounding of sea-ice thickness in the southern Sea of Okhotsk. Annals Glaciol 44:253–260. https://doi.org/10.3189/172756406781811510

Wakatsuchi M, Martin S, Munoz E (1990) Satellite and oceanographic observations of large ice-edge eddies in the Kuril Basin region of the Okhotsk Sea. Ann Glaciol 14:360–361. https://doi.org/10.3189/S026305500009381

Watanabe T, Ikeda M, Wakatsuchi M (2004) Thermohaline effects of the seasonal sea ice cover in the Sea of Okhotsk. J Geophys Res 109:C09S02. https://doi.org/10.1029/2003JC001905

Yan D, Yoshida K, Nishioka J, Ito M, Toyota T, Suzuki K (2020) Response to Sea ice melt indicates high seeding potential of the Ice Diatom Thalassiosira to spring phytoplankton blooms: a laboratory study on an ice algal community from the Sea of Okhotsk. Front Mar Sci 24:613. https://doi.org/10.3389/fmars.2020.00613